Magnetization dynamics in a dual free-layer spin-torque nano-oscillator

Graham E. Rowlands and Ilya N. Krivorotov

Phys. Rev. B **86**, 094425 — Published 20 September 2012

DOI: 10.1103/PhysRevB.86.094425

Dual Free Layer Spin Torque Oscillator

Graham E. Rowlands and Ilya N. Krivorotov*
Department of Physics and Astronomy, University of California, Irvine, California 92697

We report micromagnetic simulations of magnetization dynamics in a spin torque nano-oscillator (STNO) that consists of two in-plane free layers located between two fixed out-of-plane polarizers. In the optimal regime of the STNO operation, the free layers precess opposite one another on large-amplitude out-of-plane trajectories and generate large microwave power at the sum of their precession frequencies. Our simulations reveal that the frequency band of the STNO operation can be severely limited by formation of a static magnetic vortex in the free layers, and that the bandwidth can vanish in commonly used free layer materials such as Permalloy. We show that the vortex formation can be suppressed and the bandwidth significantly extended by increasing Gilbert damping in the free layers and minimizing coupling between the free layers by means of interlayer exchange interaction. We explore the operation of the STNO with and without the inclusion of the spin-torque coupling between the two free layers. Our simulations demonstrate that an STNO with dual free layers is a promising candidate for the development of high-power high-frequency STNOs operating in the absence of an external magnetic field.

PACS numbers: 72.25.-b,75.40.Gb,75.75.-c,75.78.Cd

Spin torque nano-oscillators (STNOs) utilize spin transfer torque (STT)[1–20] from direct spin-polarized current to excite persistent magnetization precession in magnetic multilayers, thereby generating microwave power[21–45]. If these devices are to be used for practical applications, their line widths and integrated powers must be improved[30,46]. A new type of STNO has recently been demonstrated that employs a current polarizer magnetized perpendicular to the multilayer's plane[47]. The free layer, which is located between this perpendicular polarizer and an in-plane reference layer, is pushed out of plane by STT from the polarizer whereupon it precesses on a large amplitude trajectory around the resulting easy-plane shape anisotropy field[48,49]. The continuous oscillation of the free layer with respect to the reference layer gives rise to microwave-frequency resistance and voltage oscillations by means of the giant magneto-resistance (GMR) effect between the layers[47]. Because of these increased oscillation amplitudes, this type of STNO offers a significant improvement in microwave power emission over conventional STNOs consisting of an in-plane free layer and an in-plane polarizer. The main limitation of this structure, however, is a relatively low peak frequency caused by the formation of a static vortex in the free layer at high current densities[48].

In this paper, we propose a STNO that is composed of two perpendicular polarizers and two in-plane free layers. We employ micromagnetic simulations to demonstrate that this new structure can generate large microwave power in zero external magnetic field at frequencies greater than those attainable in STNOs with a single perpendicular polarizer. Simulations show that the behavior of this STNO is strongly influenced by several considerations largely unimportant in "conventional" STNOs. While in-plane STNOs, for example, benefit from the use of free layers with low values of the Gilbert damping parameter, we find that free layers with relatively large damping are required to stave off vortex formation and enable the intended operation of the proposed dual free layer STNO. Additionally, we find that the angular asymmetry of STT, which results in either layer experiencing different out-of-plane torques, plays an important role in the behavior of the overall structure. Most importantly, one expects that the character of magnetization dynamics will depend strongly on the manner and strength of coupling between the two free layers. We therefore explore the full range of possible coupling mechanisms, starting with dipolar interactions alone and subsequently adding Néel (orange-peel) coupling and mutual STT between the layers. We show that with some combination of Néel coupling and layer-specific tuning of the damping, the bandwidth of the STNO can

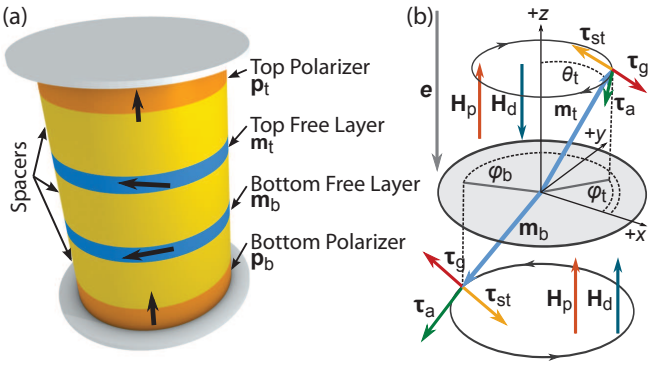

FIG. 1. (Color Online) (a) Schematic of the dual free layer STNO. (b) Torques acting on the free layers for electric current passing through the structure in the indicated direction. Torque due to the out-of-plane shape anisotropy field (τ_a) induces free layer precession around the sample's normal. Spin-torque (τ_{st}) from the polarizer adjacent to a free layer tends to increase the out-of-plane component of the free layer's magnetization, while torque due to Gilbert damping (τ_g) tends to reduce it. The directions of the demagnetization $\mathbf{H}_d$ and polarizer $\mathbf{H}_p$ fields are indicated for both layers.

be significantly increased.

The structure of the STNO with dual free layers is shown in Fig. 1(a). The device is a circular nanopillar consisting of four metallic ferromagnetic layers separated by three non-magnetic spacers made of either metals or insulating tunnel barriers. The outer layers serve as spin polarizers with unit directions $\mathbf{p}_i$ ($i = \{\text{top, bottom}\}$), while the inner layers serve as free layers with unit directions $\mathbf{m}_i$. The polarizers are composed of materials with perpendicular magnetic anisotropy sufficiently large to induce their magnetic moments to point out of the sample plane along the z-axis of the coordinate system shown in Fig. 1(b). The free layers, meanwhile, lie in the plane of the sample at equilibrium. In the presence of a direct current across the structure, one must generally analyze the full spin-dependent transport of the system. Such an analysis is beyond the scope of this paper, so we make the simplifying assumption that the magnetoresistance and STT can be analyzed independently for each pair of neighboring magnetic layers.

The operation of this new STNO proceeds as follows: assuming electrons flow through the structure in the direction indicated in Fig. 1(b), STT from the perpendicular polarizers acting on the adjacent free layers, $\boldsymbol{\tau}_{\text{st},i} \sim (\mathbf{m}_i \times (\mathbf{m}_i \times \mathbf{p}_i))$, pushes their magnetic moments towards opposite ends of the structure ($m_{z,b} < 0$, $m_{z,t} > 0$). The Gilbert damping torque, $\tau_{g,i} \sim (\mathbf{m}_i \times (\mathrm{d}\mathbf{m}_i/\mathrm{d}t))$, opposes this action and pushes the magnetizations back towards the plane. The effective fields at each layer are the sum of the easy-plane demagnetizing fields, which arise in both layers in proportion to their out-of-plane magnetization components ($\mathbf{H}_{d,i} \sim -m_{z,i}\hat{z}$), and the dipolar field from the polarizers. Consequently, the magnitude of the effective field is somewhat reduced at the top layer and enhanced at the bottom layer. The free layers' magnetic moments undergo precession around the local effective fields, and therefore do so in opposite directions around the normal to the sample plane[50]. These precessing magnetizations produce oscillations in the overall structure's resistance due to either GMR (in the case of a metallic spacer) or tunneling magnetoresistance (TMR, in the case of an insulating spacer) between the free layers. The frequency of the resistance oscillations is the sum of the individual precession frequencies of the free layers: approximately twice that attainable with a single free layer and fixed reference layer. The amplitude of the resistance oscillations is similar to the full GMR/TMR amplitude between the free layers, resulting in a large microwave power emitted from the device. We investigate the operation of this structure with and without the inclusion of the mutual STT coupling of the two free layers, $\boldsymbol{\tau}^{\text{mut}}_{\text{st},i} \sim (\mathbf{m}_i \times (\mathbf{m}_i \times \mathbf{m}_j))$. In our particular geometry this torque tends to reduce the out-of-plane component of the bottom layer while increasing the same quantity in the top free layer.

For a quantitative description of the STNO's operation, we perform micromagnetic simulations of STT driven magnetization dynamics in this structure[51]. Here we describe the results for a 50 nm diameter nanopillar with 3 nm thick free layers, 6 nm thick polarizers, and 12 nm thick GMR spacers. The discretization length for the simulations is 3 nm along the z axis and 2 nm along the other two axes. We solve the Landau-Lifshitz-Gilbert equation with STT term[1] applied to each of the free layers:

$$\frac{\mathrm{d}\mathbf{m}_i}{\mathrm{d}t} = -\gamma \mathbf{m}_i \times \mathbf{H}_i^{\text{eff}} + \alpha \left(\mathbf{m}_i \times \frac{\mathrm{d}\mathbf{m}_i}{\mathrm{d}t} \right) + \boldsymbol{\tau}_{\text{st},i}, \quad (1)$$

where $\mathbf{H}_i^{\text{eff}}$ is the total effective field acting on layer i, α is the Gilbert damping parameter, and γ is the gyromagnetic ratio. The STT term for the free layer $\mathbf{m}_i$ includes torques from both the neighboring polarizer $\mathbf{p}_i$ and the other free layer $\mathbf{m}_j$, and is given (in units of inverse seconds) by

$$\boldsymbol{\tau}_{\text{st},i} = -\gamma \frac{\hbar J_i}{|e| M_f L_f} \Big[g(\theta_i) \left[\mathbf{m}_i \times (\mathbf{m}_i \times \mathbf{p}_i) \right] - g(\theta_{ij}) \left[\mathbf{m}_i \times (\mathbf{m}_i \times \mathbf{m}_j) \right] \Big], \quad (2)$$

where e is the electron charge, L_f is the free layer thickness, M_f is the saturation magnetization of the free layers, θ_i is the angle between a free layer and its respective polarizer, and θ_{ij} is the angle between the two free layers. The angular dependence of STT is contained within $g(\theta)$, and varies depending on the choice of spacer material between the free layers. In the case of a metallic spacer, this factor can be approximated by[52]

$$g(\theta) = \frac{P\Lambda^2}{(\Lambda^2+1) + (\Lambda^2-1)\cos\theta}, \quad (3)$$

where P is the spin-polarization efficiency, and Λ is the spin torque asymmetry parameter. Meanwhile, the current density is specified as

$$J_i = J \begin{cases} +1 & i = \text{Top free layer} \\ -1 & i = \text{Bottom free layer} \end{cases}, \quad (4)$$

with opposite signs in either free layer due to the different order in which electrons traverse the two polarizer/free-layer pairs. We are interested in the resistance oscillations across this structure resulting from the dynamics described by Eqn. 1. The GMR between two layers with mutual angle θ is given in the macrospin limit by

$$R = R_0 + \Delta R \frac{\sin^2(\theta/2)}{1 + (\Lambda^2 - 1)\cos^2(\theta/2)}, \quad (5)$$

where R_0 is the base resistance and ΔR is the full scale resistance change due to GMR. Since the projections of the free layers' magnetizations on the nearest polarizers ($\mathbf{m}_i \cdot \mathbf{p}_i$) do not change over the course of the precessional trajectories, they do not contribute to the resistance oscillations across the structure. We may thus restrict our focus to the GMR between the two magnetic free layers. In the micromagnetic approach, it is typical

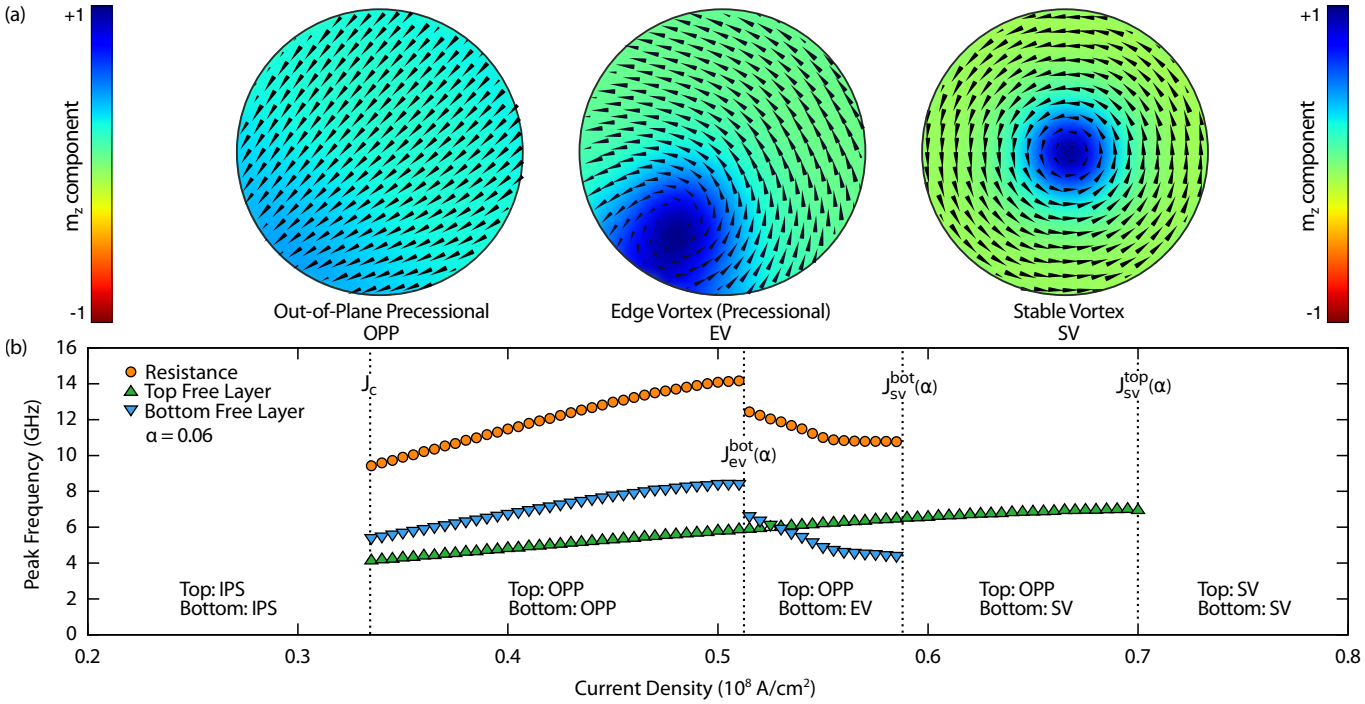

FIG. 2. (Color Online) (a) Micromagnetic states available to the bottom free layer for increasing current density. Color encodes the out-of-plane component of the normalized magnetization while the arrows represent the in-plane component. The initial in-plane static (IPS) and out-of-plane static (OPS) states are not shown. (b) Frequency behavior of the STNO as a function of applied current in the absence of the mutual STT. Resistance oscillations cease when either free layer enters the circularly symmetric stable vortex (SV) state.

to calculate the total resistance by applying, in parallel, Eqn. 5 to all pairs of computational cells situated across the GMR barrier. For the sake of convenience, we have verified that the peak frequencies of resistance oscillations may be accurately obtained simply by considering the angle between the average magnetizations of either layer. Since the free layers counterprecess with constant z-components, the angular separation of their in-plane projections φ is the only relevant quantity for the GMR oscillations of the device. This separation increases steadily as

$$\varphi = (\omega_{\rm t} + \omega_{\rm b})t, \tag{6}$$

where $\omega_{\rm t}$ and $\omega_{\rm b}$ are, respectively, the angular frequencies of the top and bottom layers. As such the resistance across the entire structure oscillates with a frequency that is the sum of the frequencies of the individual layers.

For our simulations, we assume in Eqn. 1 that the free layers have a saturation magnetization M_f = 560 emu/cm^3 and an exchange constant A =1.0×10^{-6} erg/cm. These values are typical for thin Permalloy (Ni$_{1-x}$Fe$_x$) films sandwiched between Cu layers[53]. The saturation magnetization of the polarizers, M_p, is taken to be 975 emu/cm^3 — a value similar to those of FePt and CoPt L1$_0$ alloys exhibiting strong perpendicular magnetic anisotropy[54,55]. The spin-polarization and STT asymetry are taken to be P = 0.22 and Λ = 1.8 in the polarizers and P = 0.15 and Λ = 1.4 in the free layers (when the mutual torque is taken into account). The magnetizations of the polarizing layers are assumed to be spatially uniform and fixed perpendicular to the sample plane; their dipolar field, while slightly nonuniform, points mostly in the z direction and is roughly 1.1 kOe in magnitude. The Oersted field resulting from the electric charge current impacts magnetic vortex formation and stability, and is therefore included. We find that the Gilbert damping parameter, α, has a strong impact on the dynamics exhibited by the STNO with dual free layers, and thus we study the system as α is varied over the 0.007–0.1 range. Such control of the free layer damping can be realized in practice by doping the free layer with Tb, though the resistivity of the Permalloy is increased and the GMR ratio slightly decreased in the process[56,57].

Fig. 2(a) shows, in the absence of the mutual STT, the sequence of micromagnetic states assumed by the bottom free layer as a function of increasing current density. The set of realizable states depends strongly on the character of the local effective field, which differs substantially between the free layers. The stray field from the perpendicular polarizers, for example, points in the $+z$ direction while the magnetizations of the top and bottom free layers are pulled towards $+z$ and $-z$ respectively. As a result of these asymmetries, the top free layer only passes through a subset of states assumed by the bottom free layer as the current density increases.

The dependence of the oscillator frequency on applied

current density, again in the absence of the mutual STT, is shown in Fig. 2(b) for a $\alpha = 0.06$. At zero current, the ground state of the system is an anti-parallel in-plane static (IPS) configuration of the free layers stabilized by their dipolar coupling. The IPS state is destabilized simultaneously in both layers when this coupling is overcome at a critical current density, $J_c = 0.34 \times 10^8$ A/cm^2, that is in accord with values found from simulations performed for STNOs with a single perpendicular polarizer[47–49]. This critical current density is independent of the Gilbert damping, and is determined primarily by the magnitude of the precessional torque resulting from dipolar coupling between the free layers. For $J > J_c$, both layers follow out-of-plane precessional (OPP) trajectories as shown in Fig. 1(b), though the bottom layer's magnetization precesses more rapidly than that of the top layer despite possessing a smaller $|m_z|$. Simulations indicate that this asymmetry arises from the angular dependence of STT, $g(\theta_i)$, which results in the bottom layer being displaced further from its energy minimum and thus being subjected to a larger effective field. If the asymmetry $\Lambda \to 0$, there is no appreciable difference in the frequencies of the two layers. At a larger current density, J_{ev}, we observe the nucleation of a vortex in the bottom layer whose core reaches a limit cycle at a radius R_c from the center of the disk. This edge vortex (EV) remains in the state of persistent gyration at the same radius R_c for modest increases in the current density, but at some yet larger current density J_{sv}^{bot} the EV abruptly spirals inward to become a stable vortex (SV) at the center of the free layer. Since the bottom free layer enters a circularly symmetric state at this current density, the resistance oscillations across the structure cease even though the top free layer remains in the dynamic OPP state. The EV state is not observed in the upper free layer. Instead, at a higher current density J_{sv}^{top}, the top layer passes directly from the OPP state into the SV state owing to a different local field at that layer. At yet higher current densities both layers ultimately pass into the out-of-plane static (OPS) state with $|m_z| \approx 1$.

If we now include the mutual STT between the two layers, we find that the behavior of the STNO is simplified as seen in Fig. 3. This new torque favors a so-called "windmill" behavior of the free layers in which they both precess in the same direction with some relative phase. This tendency is contrary to the counter-precessional motion induced by the demagnetizing fields, and hence the critical current J_c is modestly increased. As one of the layers undergoes a transition into a micromagnetic state, the resulting inter-layer torque becomes similarly nonuniform and the other free layer soon thereafter undergoes a transition of its own. This behavior sees the elimination of the EV phase and the simultaneous transition of both layers to the SV state at $J_{sv}^{top} = J_{sv}^{bot}$. We also observe that the frequencies of the two free layers have become comparable. This is expected, since the bottom free layer is pulled towards the top free layer while the top layer is pushed away from the bottom. Thus, the spin torque

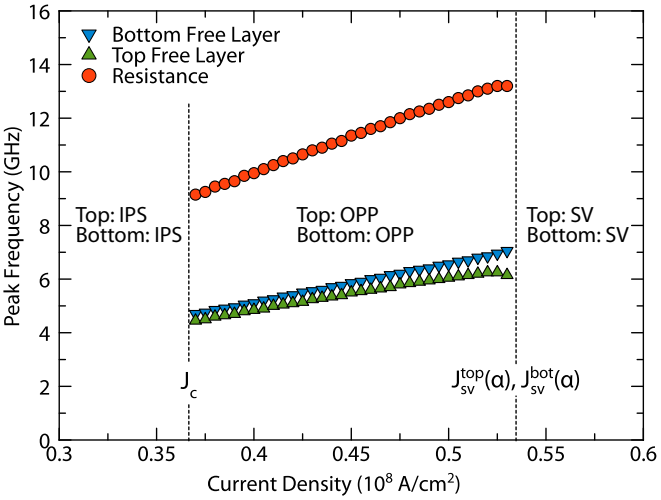

FIG. 3. (Color Online) Frequency behavior in the presence of the mutual STT between the magnetic free layers. The simulation is conducted with $\alpha = 0.06$.

asymmetry is counteracted and the frequencies converge. For similar reasons, we see a decrease in the maximum frequency of resistance oscillations.

The behaviors shown in Figs. 2(b) and 3 only reflect the evolution of the STNO states for a single choice of damping α. One might expect that variations in α would simply rescale the critical currents without altering the qualitative behavior of the STNO. This is not the case, however, since J_c (determined by the coupling between the free layers) is independent of α[38]. Indeed, in the limit of $\alpha \to 0$, all critical current densities except for J_c tend to zero, and once J reaches J_c, the free layer directly undergoes the IPS→OPS state completely bypassing the OPP, EV and SV states. It follows that in order for the STNO to act as a microwave voltage source, the damping must be large enough to increase the critical current for vortex formation to a value exceeding J_c.

The strong dependence of the available micromagnetic states on the Gilbert damping in the free layers prompts us to study the STNO behavior as a function of the free layer damping. The current-damping phase diagrams summarizing our micromagnetic simulations are shown in Fig. 4, and are constructed for current densities ramped slowly from zero. In contrast to simply providing a scaling effect, we observe that larger values of α facilitate the emergence of otherwise inaccessible states. In the case of no mutual STT between the layers, we observe that for sufficiently small values of the damping parameter $\alpha < \alpha_1$ shown in Fig. 4(a), the system moves directly from the IPS state into SV states in both the bottom and top free layers at J_c. For higher damping, $\alpha_1 < \alpha < \alpha_2$, the top layer moves from IPS into OPP at J_c, while the bottom layer still switches directly into the SV state. For $\alpha_2 < \alpha < \alpha_3$ the bottom layer moves from IPS to EV, and for $\alpha > \alpha_3$ the bottom layer moves directly into the OPP state. Only at elevated damping values

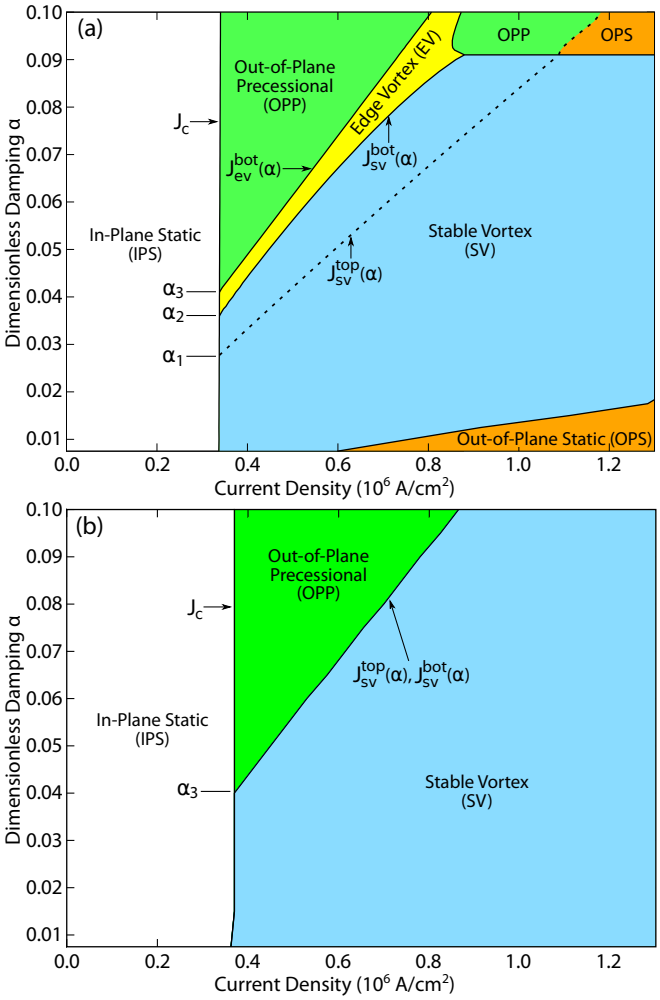

FIG. 4. (Color Online) (a) Phase diagram for the STNO in current-damping space in the absence of the mutual STT. Labels indicate the state of the bottom free layer, while the dotted line gives the OPP→SV transition of the top free layer (OPP to the left and SV to the right of the line). (b) Phase diagram in the presence of the mutual STT. Both free layers now occupy the same states at all points on the diagram. These diagrams are constructed for current densities ramped slowly from J=0. All transitions are first order.

($\alpha > \alpha_3 = 0.04$) do we observe both layers precessing simultaneously in the OPP phase (the desired mode of operation of the STNO). At $\alpha > 0.09$, we see a reentrant OPP phase in the bottom layer that takes the place of the SV phase. If we now include the mutual STT between the layers the diagram is much simplified as seen in Fig. 4(b): both free layers now occupy the same states at all points on the phase diagram, and the EV phase is no longer available to the either layer.

Once the current has been ramped up enough to establish the SV phase in both layers, we study the available steady states of the system as a function of decreasing current. As the current density decreases, the transitions between the STNO phases take place in the reverse order at lower current densities than the corresponding transitions during ramp-up. This hysteretic nature of the phase transitions confirms that they are first order, and thus that there are regions of phase space where more than a single state of the system is stable. At non-zero temperatures we expect that thermal noise will induce random transitions between these states, potentially increasing the linewidth of the STNO. We find, however, that for a sufficiently large damping parameter ($\alpha > 0.08$), there is a region of the OPP phase (not pictured in Fig. 4) where there is no bistability with the SV or EV states. In this region, we can rely on high-power precessional STNO operation.

Fig. 5(a) shows the dependence of the oscillator frequency on current for three values of the Gilbert damping parameter of the free layers. It is clear that the lower frequency bound of the oscillations decreases with increasing damping. The dependence of the STNO frequency on damping follows from the approximate relation (which becomes exact in the macrospin approximation) expressing balance between ST and damping torque in the OPP state:

$$\alpha\langle H_{z,i}\rangle = aJ\langle g(\theta_i,\eta)\rangle, \tag{7}$$

where $\langle H_{z,i}\rangle = 4\pi N_z\langle M_{f,z,i}\rangle + \langle H_{z,i}\rangle$ is the absolute value of the spatial average of the z-component of the net effective field acting on the i-th free layer, $M_{f,z,i} = M_f\cos\theta_i$ is the z-component of the free layer magnetization, N_z is the z-axis demagnetization factor, $H_{z,i}$ is the z-component of the net magnetic field from the polarizers and the other free layer, and $a = \hbar/(2eM_fL_f)$. Eqn. 7 follows from Eqn. 1 and states that the out-of-plane angle of the precessing magnetization is determined by the competition between STT and Gilbert damping as illustrated in Fig. 1(b). Since the free layer precession frequency in the OPP state is approximately proportional to $\langle H_{z,i}\rangle$, the frequency of precession at J_c decreases with increasing α as predicted by Eqn. 7 and confirmed by micromagnetic simulations (see Fig. 5(a)).

Potential device applications motivate us to consider means by which we can increase the bandwidth of the STNO. This, by definition, involves some combination of decreasing the lower frequency bound and increasing the upper frequency bound. We have already identified the dipolar coupling between free layers as the origin of the critical current J_c, and reduction of this quantity should afford us a smaller value of $\langle H_{z,i}\rangle$, and thus a smaller generation frequency at $J = J_c$. The high frequency cutoff requires a more detailed analysis. The upper end of the STNO frequency band (14 GHz) does not, as seen in Fig. 5(a), depend on α. The highest operation frequency is found at the point of the OPP→EV transition in the bottom free layer, during which the free layer's demagnetization energy is reduced from that in the OPP state (e.g. $\langle M_{f,z,\mathrm{bot}}\rangle$ is reduced from -0.38 to -0.31 for $\alpha = 0.075$). We assume that, for a given value of M_f, the OPP→EV transition takes place when the average out-of-plane component of the free layer magnetization

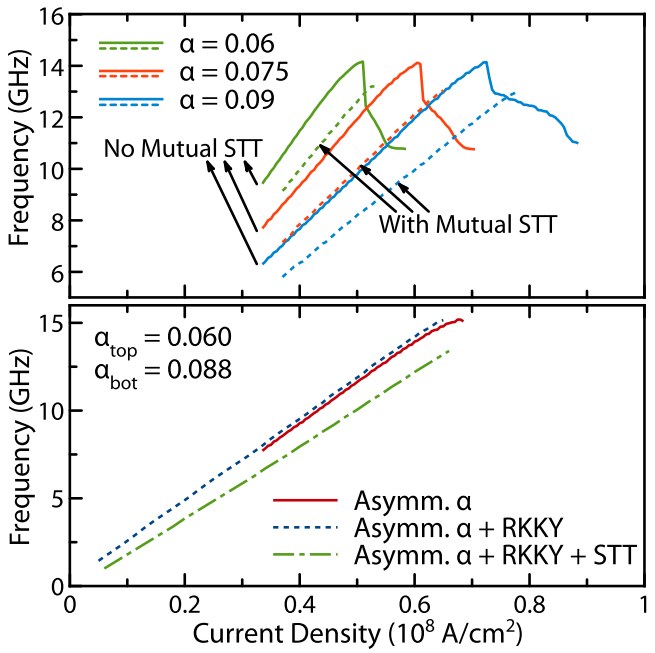

FIG. 5. (Color Online) (a) Frequency of the resistance oscillations for three values of α (identical in both free layers). The dotted lines are for simulations where the mutual STT was included. (b) Frequency of the resistance oscillations for $\alpha_{top} = 0.060$ and $\alpha_{bot} = 0.088$. The solid line includes neither the mutual STT nor the ferromagnetic coupling, the dotted line includes a ferromagnetic coupling as discussed in the text, and the dot-dashed line also includes the mutual torque between the layers.

$\langle M_{f,z,\mathrm{bot}} \rangle$, and hence the average demagnetizing field, exceeds some critical value independent of α. Since the demagnetizing field can be parameterized by the magnetization's polar angle θ, we can estimate the critical angle θ_{ev} at which the transition occurs using Eqn. 7 and the phase diagram in Fig. 4. Starting from the balance between STT and the damping in the OPP state given by Eq.(7), we arrive at an expression for $J_{\mathrm{ev}}(\alpha)$:

$$J_{\mathrm{ev}}(\alpha) = \alpha \left(\frac{4\pi M_f N_z \langle \cos(\theta_{\mathrm{ev}}) \rangle + \langle H_{z,i} \rangle}{a \langle g(\theta_{\mathrm{ev}}, \eta) \rangle} \right). \quad (8)$$

Substituting $\cos(\theta_{\mathrm{ev}})$ for $\langle \cos(\theta_{\mathrm{ev}}) \rangle$ and $g(\theta_{\mathrm{ev}}, \eta)$ for $\langle g(\theta_{\mathrm{ev}}, \eta) \rangle$ in Eq.(8), and fitting Eq.(8) to the $J_{\mathrm{ev}}(\alpha)$ phase boundary on the phase diagram in Fig. 4 with θ_{ev} as the fitting parameter, we can estimate θ_{ev}. Though a rough estimate of this angle can be obtained by neglecting the $\langle H_{z,i} \rangle$ term, we include the value of $\langle H_{z,i} \rangle = 1.1$ kOe extracted directly from the micromagnetic simulations into the fit. In the case of $\alpha = 0.075$, the fit gives $\theta_{\mathrm{ev}} = 110°$ (from the $+\hat{z}$ direction, only 20° below the plane). In good agreement with this prediction, and standing as confirmation that the demagnetizing field is the dominant factor in determining the critical currents for vortex formation, the average value $\langle \theta_{\mathrm{ev}} \rangle$ as obtained from our simulations just before the OPP→EV transition is found to be 113°.

As Fig. 5(a) demonstrates, increasing the damping is one method of extending the lower frequency bound of the STNO operation. As mentioned above, suppression of the critical current J_c should allow us to attain a smaller generation frequency at $J = J_c$. Such a reduction of J_c can be implemented by use of magnetic materials with smaller M_f, which reduces the magnetostatic coupling between the free layers. The reduction of M_f could also alter the upper frequency bound by decreasing the demagnetization energy and thereby impeding vortex formation. Simulations reveal that this effect, while evident, only results in a marginal increase in the maximum STNO frequency ($< 5\%$). While the critical out-of-plane angle for vortex formation θ_{ev} (as treated below) increases with decreasing M_f, the frequency of precession at this angle stays nearly the same since the product of M_f and $\cos(\theta_{\mathrm{ev}})$ (which determines the frequency of precession at the critical angle) is nearly independent of M_f.

Another promising approach for reducing the effective coupling between the free layers is the introduction of interlayer coupling favoring a parallel free layer alignment at zero current. Such a coupling can be generated by either an RKKY interaction[58] or a Néel coupling originating from the correlated surface roughness of the magnetic layers[59,60]. The magnitude of the RKKY coupling can be tailored through adjustment of the metallic GMR spacer thickness between the free layers, and can be chosen to nearly cancel the dipolar coupling between them. In this case the effective coupling between the free layers will be nearly zero, resulting in a very low critical current density J_c and a wide operation bandwidth even for small Gilbert damping. In this regime, the critical current J_c will likely be determined by residual in-plane anisotropy resulting from deviations of the nanopillar shape from a perfectly circular cross-section. This method also allows the thickness of the GMR spacer to be significantly reduced, as the relatively high 12 nm spacer thickness for the studied STNO structure was chosen to reduce the dipolar coupling by means of increasing the spatial separation of the free layers. For this particular simulation, the spacer thickness is reduced from 12 nm to 3 nm, an approximate value for which ferromagnetic RKKY coupling of the required magnitude can be achieved for a metallic spacer layer. As seen in Fig. 5(b) the ferromagnetic interlayer coupling reduces the lower frequency bound of the STNO to nearly 1 GHz, resulting in a substantial increase in the oscillator bandwidth.

The upper frequency range of the STNO can be increased by tuning the damping parameters independently in either free layer such that both layers reach the critical value of $\langle M_{f,z,i} \rangle$ at the same current density. As mentioned earlier, the asymmetric angular dependence of STT causes the magnitude of STT acting on the bottom free layer to exceed that acting on the top. If the damping in the bottom layer is elevated to the appropriate value, this effect can be balanced and both layers will

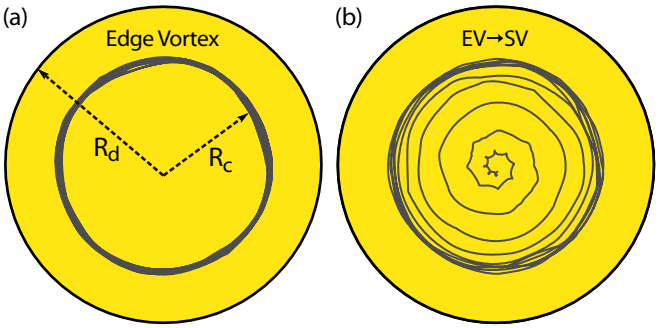

FIG. 6. (Color Online) The trajectories traced out by the vortex core in the bottom free layer at $\alpha = 0.075$ (a) as the core orbits at radius R_c in the EV state at J=0.705×10^8 A/cm^2 and (b) as the core spirals to the center of the disk during the EV→SV transition at J=0.710 10^8 A/cm^2. The radius is the disk is shown at R_d. Deviations from a circular trajectory are due to dipolar coupling to the top free layer precessing in the OPP state.

undergo vortex transitions at identical current densities corresponding to their respective maximum precessional frequencies. Fig. 5(b) illustrates this method of increasing the STNO operation frequency: choosing $\alpha = 0.088$ in the bottom layer and $\alpha = 0.060$ in the top results in a maximum generation frequency of 15 GHz, which is an improvement over the 14 GHz maximum frequency attainable for equal values of α in both free layers. Fig. 5(b) demonstrates the widest bandwidth we were able to obtain by including a ferromagnetic interlayer exchange coupling as well tuning the damping in either layer.

It is apparent that free layer vortex formation is the main factor limiting high-frequency operation of the dual free layer STNO, thus we strive to understand the factors promoting vortex nucleation. Vortices on a 50 nm diameter, 3 nm thick Py disk are not stable at zero current[61], and at $T = 0$ are only accessible through the action of STT and/or external fields. The Oersted field from the electric charge current through the nanopillar serves as a stabilizing magnetostatic field for vortices of the appropriate chirality, since it shares its circular symmetry with the SV state. Our simulations show, however, that the Oersted field is not a significant factor promoting vortex formation in 50 nm diameter nanopillars.

While the demagnetizing field is the primary driving force of the OPP→EV transition (vortex nucleation), the nature of the EV→SV transition is less transparent. We plot in Fig. 6 the trajectory of the vortex core immediately before and after the transition. In order to extract the location of the core we first generate a perfectly circular in-plane vector field around an initial guess for the core's coordinates (x_0,y_0), and then calculate the difference of this field from the actual in-plane magnetization profile. We then minimize the square of this difference by varying the guess for the core location until convergence.

We observe that the nucleated vortex core moves, as shown in Fig. 6(a), to a limit cycle at a radius R_c (the

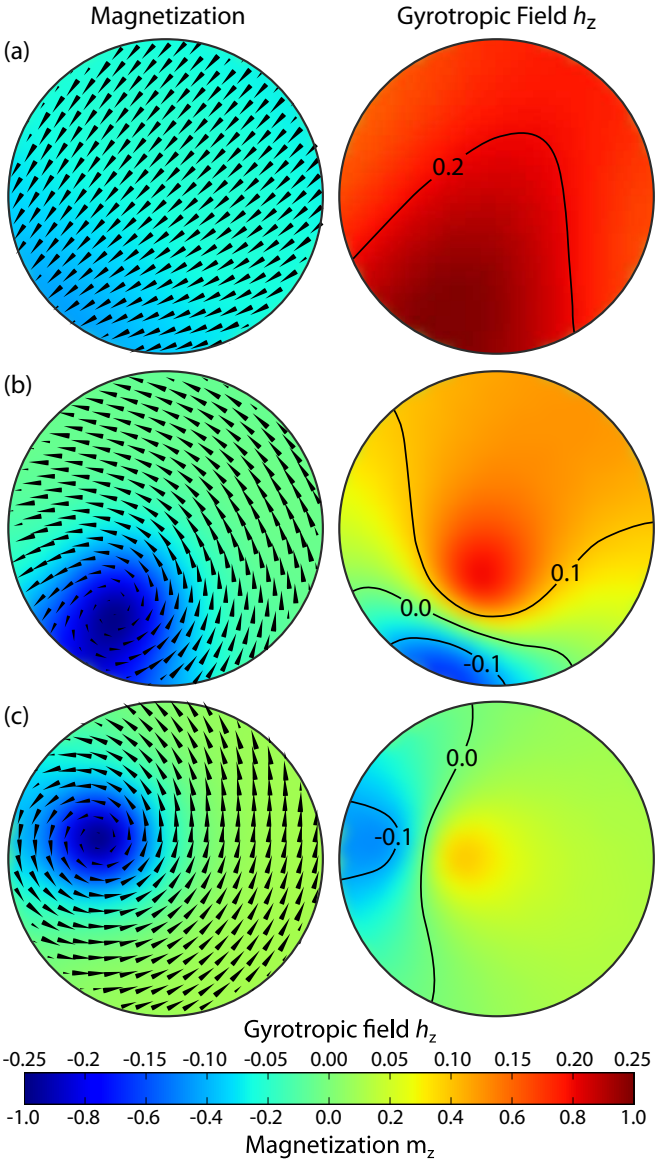

FIG. 7. (Color Online) The magnetization profiles with the in-plane component shown by arrows and m_z encoded by color (left column) and normal components of the gyrotropic field, $h_z(x, y)$ (right column), displayed for the bottom free layer (a) in the OPP phase at $J = 0.6\ 10^8$A/cm^2, (b) the EV phase at $J = 0.860\ 10^8$A/cm^2, and (c) during the EV→SV transition at $J = 0.865\ 10^8$A/cm^2. All figures shown are for $\alpha = 0.09$.

EV state) where it remains impervious to increases of the current density in the J_{ev} to J_{sv} range before it spirals as shown in Fig. 6(b) to the center of the disk. Despite being topologically distinct, the behavior of the vortex in the EV state is very similar to that seen in the dynamic state of two coupled edge solitons studied numerically in Ref. 62 on Permalloy discs large enough to support the SV state at zero current. To elucidate the origin of the EV→SV transition, we examine the profile of the gyrotropic field: the effective field derived from the kinetic contributions to the total energy[63,64]. We are pri-

marily interested in the normal component, h_z, which is known to drive the vortex core reversal in larger magnetic disks[65,66]:

$$h_z = -\frac{1}{\gamma}\left(\mathbf{m} \times \frac{\mathrm{d}\mathbf{m}}{\mathrm{d}t}\right)_z . \quad (9)$$

Snapshots of $h_z(x, y)$ for the bottom free layer are shown in Fig. 7 for the steady-state OPP and EV phases of the oscillator as well as for the initial stage of the EV→SV transition. In Fig. 7(a), the OPP phase yields an $h_z(x, y)$ that is positive throughout the free layer, which simply reflects the tendency of the damping to move the quasi-uniform magnetization of the free layer back into the plane of the sample. In the EV phase, as pictured in Fig. 7(b), h_z develops a negative region at the edge of the disk. This negative h_z drives the nucleation of the edge vortex. Note that the bulk of the bottom free layer magnetization develops a small positive out-of-plane component in the EV state, which is a result of the polarizers' stray field favoring a positive z-component of the free layers' magnetizations. With increasing current, the magnetization profile in the EV state continues to smoothly deform (while the negative h_z region continues to increase in size) until the vortex core abruptly begins to move inward from R_c at $J = J_{sv}$, as shown in Fig. 7(c). During this transition we observe a concurrent reduction of the magnitude of h_z since the fully nucleated vortex carries the polarity favored by the applied STT[62].

In conclusion, we have numerically studied the properties of a spin torque nano-oscillator with two perpendicular polarizers and two free layers. In the optimal regime of operation, the magnetizations of both free layers are quasi-uniform and precess on large-amplitude out-of-plane trajectories. Since the magnetizations counter-precess, the oscillator can generate a large-amplitude high-frequency microwave signal. We observe that the mutual STT acting between the free layers does not qualitatively alter the precessional state of the system, but does have a strong impact on the system once it develops a substantial micromagnetic curvature. Our simulations indicate that the main limiting factor of the operation of this type of spin torque oscillator is magnetic vortex formation in the free layers. We determine several means of suppressing the vortex formation and thereby improving the overall performance of the oscillator: (i) increasing the free layer damping, (ii) decreasing coupling between the free layers via control of the interlayer exchange coupling and (iii) selective control of Gilbert damping in the free layers. We show that with these optimizing factors implemented, the dual free layer spin torque oscillator with Tb-doped Permalloy free layers can operate in the 1–15 GHz frequency band and show excellent linearity of the generation frequency with the applied current.

The authors thank E. Fullerton, J. Katine, A. Slavin, and V. Tiberkevich for many useful discussions. This work was supported by NSF Grants No. DMR-0748810 and No. ECCS-1002358 and by the Nanoelectronics Research Initiative through the Western Institute of Nanoelectronics. Computations supporting this paper were performed on the BDUC Compute Cluster donated by Broadcom, co-run by the UCI OIT and the Bren School of Information and Computer Sciences.

* ilya.krivorotov@uci.edu

[1] J. C. Slonczewski, J. Magn. Magn. Mater. **159**, L1 (1996).
[2] L. Berger, Phys. Rev. B **54**, 9353 (1996).
[3] J. A. Katine, F. J. Albert, R. A. Buhrman, E. B. Myers, and D. C. Ralph, Phys. Rev. Lett. **84**, 3149 (2000).
[4] M. Tsoi, A. Jansen, J. Bass, W. Chiang, V. Tsoi, and P. Wyder, Nature **406**, 46 (2000).
[5] J. Grollier, V. Cros, A. Hamzic, J. M. George, H. Jaffres, A. Fert, G. Faini, J. Ben Youssef, and H. Legall, Appl. Phys. Lett. **78**, 3663 (2001).
[6] S. Urazhdin, N. O. Birge, W. P. Pratt, and J. Bass, Phys. Rev. Lett. **91**, 146803 (2003).
[7] S. Kaka, M. R. Pufall, W. H. Rippard, T. J. Silva, S. E. Russek, and J. A. Katine, Nature **437**, 389 (2005).
[8] F. B. Mancoff, N. D. Rizzo, B. N. Engel, and S. Tehrani, Nature **437**, 393 (2005).
[9] A. Ruotolo, V. Cros, B. Georges, A. Dussaux, J. Grollier, C. Deranlot, R. Guillemet, K. Bouzehouane, S. Fusil, and A. Fert, Nature Nanotech. **4**, 528 (2009).
[10] X. Jiang, L. Gao, J. Z. Sun, and S. S. P. Parkin, Phys. Rev. Lett. **97**, 217202 (2006).
[11] Y. B. Bazaliy, B. A. Jones, and S.-C. Zhang, Phys. Rev. B **57**, R3213 (1998).
[12] X. Waintal, E. B. Myers, P. W. Brouwer, and D. C. Ralph, Phys. Rev. B **62**, 12317 (2000).
[13] J. Z. Sun, Phys. Rev. B **62**, 570 (2000).
[14] M. D. Stiles and A. Zangwill, Phys. Rev. B **66**, 014407 (2002).
[15] J. Fernández-Rossier, M. Braun, A. S. Núñez, and A. H. MacDonald, Phys. Rev. B **69**, 174412 (2004).
[16] Z. Li and S. Zhang, Phys. Rev. B **68**, 024404 (2003).
[17] D. M. Edwards, F. Federici, J. Mathon, and A. Umerski, Phys. Rev. B **71**, 054407 (2005).
[18] S. M. Rezende, F. M. de Aguiar, and A. Azevedo, Phys. Rev. Lett. **94**, 037202 (2005).
[19] Y. Tserkovnyak, A. Brataas, G. E. W. Bauer, and B. I. Halperin, Rev. Mod. Phys **77**, 1375 (2005).
[20] I. Theodonis, N. Kioussis, A. Kalitsov, M. Chshiev, and W. H. Butler, Phys. Rev. Lett. **97**, 237205 (2006).
[21] S. I. Kiselev, J. C. Sankey, I. N. Krivorotov, N. C. Emley, R. J. Schoelkopf, R. A. Buhrman, and D. C. Ralph, Nature **425**, 380 (2003).
[22] W. H. Rippard, M. R. Pufall, S. Kaka, S. E. Russek, and T. Silva, Phys. Rev. Lett. **92**, 027201 (2004).
[23] M. Covington, M. AlHajDarwish, Y. Ding, N. J. Gokemeijer, and M. A. Seigler, Phys. Rev. B **69**, 184406 (2004).
[24] I. K. Yanson, Y. G. Naidyuk, D. L. Bashlakov, V. V. Fisun, O. P. Balkashin, V. Korenivski, A. Konovalenko, and R. I. Shekhter, Phys. Rev. Lett. **95**, 186602 (2005).
[25] O. Boulle, V. Cros, J. Grollier, L. G. Pereira, C. Deranlot,

F. Petroff, G. Faini, J. Barnaś, and A. Fert, Nature Phys. **3**, 492 (2007).
[26] V. S. Pribiag, I. N. Krivorotov, G. D. Fuchs, P. M. Braganca, O. Ozatay, J. C. Sankey, D. C. Ralph, and R. A. Buhrman, Nature Phys. **3**, 498 (2007).
[27] A. M. Deac, A. Fukushima, H. Kubota, H. Maehara, Y. Suzuki, S. Yuasa, Y. Nagamine, K. Tsunekawa, D. D. Djayaprawira, and N. Watanabe, Nature Phys. **4**, 803 (2008).
[28] R. Lehndorff, D. Bürgler, S. Gliga, R. Hertel, P. Grünberg, C. Schneider, and Z. Celinski, Phys. Rev. B **80**, 054412 (2009).
[29] P. K. Muduli, Y. Pogoryelov, S. Bonetti, G. Consolo, F. Mancoff, and J. Akerman, Phys. Rev. B **81**, 140408(R) (2010).
[30] P. M. Braganca, B. A. Gurney, B. A. Wilson, J. A. Katine, S. Maat, and J. R. Childress, Nanotechnology **21**, 235202 (2010).
[31] T. Devolder, J.-V. Kim, M. Manfrini, W. van Roy, L. Lagae, and C. Chappert, Appl. Phys. Lett. **97**, 072512 (2010).
[32] X. Cheng, C. T. Boone, J. Zhu, and I. N. Krivorotov, Phys. Rev. Lett. **105**, 047202 (2010).
[33] V. Demidov, S. Urazhdin, and S. Demokritov, Nat. Mater. **9** (2010).
[34] G. Bertotti, C. Serpico, I. D. Mayergoyz, A. Magni, M. DAquino, and R. Bonin, Phys. Rev. Lett. **94**, 127206 (2005).
[35] M. A. Hoefer, M. J. Ablowitz, B. Ilan, M. R. Pufall, and T. J. Silva, Phys. Rev. Lett **95**, 267206 (2005).
[36] A. Slavin and V. Tiberkevich, Magnetics, IEEE Transactions on **45**, 1875 (2009).
[37] B. Montigny and J. Miltat, J. Appl. Phys. **97**, 10C708 (2005).
[38] X. Wang, G. E. W. Bauer, and A. Hoffmann, Phys. Rev. B **73**, 054436 (2006).
[39] M. Gmitra and J. Barnas, Phys. Rev. Lett. **99**, 097205 (2007).
[40] K.-J. Lee, A. Deac, O. Redon, J.-P. Nozières, and B. Dieny, Nat. Mater. **3**, 877 (2004).
[41] X. Zhu and J. G. Zhu, IEEE T. Magn. **42**, 2670 (2006).
[42] G. Finocchio, I. N. Krivorotov, M. Carpentieri, G. Consolo, B. Azzerboni, L. Torres, E. Martinez, and L. Lopez-Diaz, J. Appl. Phys. **99**, 08G507 (2006).
[43] D. V. Berkov, C. T. Boone, and I. N. Krivorotov, Phys. Rev. B **83**, 054420 (2011).
[44] B. A. Ivanov and C. E. Zaspel, Phys. Rev. Lett. **99**, 247208 (2007).
[45] A. V. Khvalkovskiy, J. Grollier, A. Dussaux, K. A. Zvezdin, and V. Cros, Phys. Rev. B **80**, 140401(R) (2009).
[46] J. A. Katine and E. E. Fullerton, J. Magn. Magn. Mater. **320**, 1217 (2008).
[47] D. Houssameddine, U. Ebels, B. Delaet, B. Rodmacq, I. Firastrau, F. Ponthenier, M. Brunet, C. Thirion, J.-P. Michel, L. Prejbeanu-Buda, M.-C. Cyrille, O. Redon, and B. Dieny, Nat. Mater. **6**, 441 (2007).
[48] I. Firastrau, D. Gusakova, D. Houssameddine, U. Ebels, M.-C. Cyrille, B. Delaet, B. Dieny, O. Redon, J.-C. Toussaint, and L. D. Buda-Prejbeanu, Phys. Rev. B **78**, 024437 (2008).
[49] U. Ebels, D. Houssameddine, I. Firastrau, D. Gusakova, C. Thirion, B. Dieny, and L. D. Buda-Prejbeanu, Phys. Rev. B **78**, 024436 (2008).
[50] A. D. Kent, B. Özyilmaz, and E. del Barco, Appl. Phys. Lett. **84**, 3897 (2004).
[51] M. Donahue and D. Porter, "OOMMF User's Guide, Version 1.0," (1999).
[52] J. C. Slonczewski, J. Magn. Magn. Mater. **247**, 324 (2002).
[53] C. Boone, J. A. Katine, J. R. Childress, J. Zhu, X. Cheng, and I. N. Krivorotov, Phys. Rev. B **79**, 140404(R) (2009).
[54] T. Seki, T. Shima, K. Takanashi, Y. Takahashi, and E. Matsubara, Appl. Phys. Lett. **82**, 2461 (2003).
[55] H. Zeng, M. L. Yan, N. Powers, and D. J. Sellmyer, Appl. Phys. Lett. **80**, 2350 (2002).
[56] W. Bailey, P. Kabos, F. Mancoff, and S. E. Russek, IEEE T. Magn. **37**, 1749 (2001).
[57] S. E. Russek, P. Kabos, R. D. McMichael, C. G. Lee, W. E. Bailey, R. Ewasko, and S. C. Sanders, J. Appl. Phys. **91**, 8659 (2002).
[58] S. S. P. Parkin, N. More, and K. P. Roche, Phys. Rev. Lett. **64**, 2304 (1990).
[59] L. Néel, C. R. Acad. Sci., Paris **255**, 1676 (1962).
[60] B. D. Schrag, A. Anguelouch, S. Ingvarsson, G. Xiao, Y. Lu, P. L. Trouilloud, A. Gupta, R. A. Wanner, W. J. Gallagher, P. M. Rice, and S. S. P. Parkin, Appl. Phys. Lett. **77**, 2373 (2000).
[61] K. Metlov, J. Magn. Magn. Mater. **242–245**, 1015 (2002).
[62] K.-S. Lee, M.-W. Yoo, Y.-S. Choi, and S.-K. Kim, Phys. Rev. Lett. **106**, 147201 (2011).
[63] W. Döring, Z. Naturforsch **3a**, 373 (1948).
[64] A. A. Thiele, Phys. Rev. Lett. **30**, 230 (1973).
[65] K. Yamada, S. Kasai, Y. Nakatani, K. Kobayashi, H. Kohno, A. Thiaville, and T. Ono, Nat. Mater. **6**, 269 (2007).
[66] K. Y. Guslienko, K.-S. Lee, and S.-K. Kim, Phys. Rev. Lett. **100**, 027203 (2008).